CFD analysis of the squeeze film damping mechanism in the first stage of servovalves

Cite as: AIP Conference Proceedings **2191**, 020145 (2019); https://doi.org/10.1063/1.5138878
Published Online: 17 December 2019

Paolo Tamburrano, Andrew R. Plummer, Phil Elliott, Pietro De Palma, Elia Distaso, and Riccardo Amirante

CFD analysis of the squeeze film damping mechanism in the first stage of servovalves

Paolo Tamburrano[1,2, a)], Andrew R. Plummer[2)], Phil Elliott[3)], Pietro De Palma[1)], Elia Distaso[1)] and Riccardo Amirante[1)]

[1] *Department of Mechanics, Mathematics and Management (DMMM), Polytechnic University of Bari, Bari, Italy*
[2]*Centre for Power Transmission and Motion control (PTMC), University of Bath, Bath, UK*
[3] *Moog Controls Ltd, Aircraft Group, Tewkesbury, UK.*

[a)]*Corresponding author: paolo.tamburrano@poliba.it*

Abstract. A fundamental component of two-stage servovalves is the flexure tube, since it both constitutes a low friction pivot for the inner flapper and allows the torque motor to be separated from the hydraulic fluid, thus avoiding contamination particles being trapped inside the torque motor. The inertia of the torque motor armature interacting with the flexure tube stiffness gives lightly damped resonances, which may lead to fatigue failure due to excessive bending under vibration, as well as limiting the position control bandwidth of the main spool. This effect is counteracted by the film of liquid interposed between the flapper and the flexure tube, which is "squeezed" during the flapper motion providing damping. However, the underlying physics of the damping mechanism caused by the squeeze film inside the flapper-flexure tube system is not well-understood, and to date the scientific literature has lacked analyses and investigations aimed at providing insights into this phenomenon. Because of this, the aim of this paper is to develop a reliable CFD model which can help to understand where and how the damping forces are generated during the flapper motion because of the squeeze film. The developed model could be used in further investigations, aimed, for example, at studying the effects of fluid properties and geometric parameters upon the damping factor, in order to achieve more effective designs which can enhance the damping factor in the flapper-flexure tube system of new generation servovalves.
This work has been carried out as a collaboration between the University of Bath and the Polytechnic University of Bari, and Moog Controls ltd (Tewkesbury, UK), a world leading manufacturer of servovalves.

INTRODUCTION

Electro-hydraulic servovalves are widely used components in the aerospace and industrial sectors because of their reliability and high-performance levels [1]. Because servovalves have the capability of providing a continuous variation of flow with high dynamics according to an input signal by using a sliding spool as the control element, they constitute key components for closed-loop electro-hydraulic motion control systems. They are also a vital part of aircraft control systems, being used for engine fuel control, brake and steering control, and for primary flight controls (actuation of elevators, ailerons and rudders), and number about 40 on a typical airliner [2].

The most common architecture is composed of two stages (a main stage and a pilot stage), in which the pilot stage (also called the first stage) works as a hydraulic amplifier interposed between the electrical input and the main stage (also called the second stage) which usually employs a sliding spool. The hydraulic amplifier, which can be a double nozzle-flapper, a jet pipe or a deflector jet, generates a force imbalance on the extremities of the main stage spool which is forced to move and in turn allows flow modulation [2]. Fig. 1 shows the architectures of these servovalves. The electrical input is represented by the current supplied to the coils of the torque motor, which in turns moves the flapper; the flapper moves inside a fundamental component, namely, the flexure tube, which provides a lightweight

74th ATI National Congress
AIP Conf. Proc. 2191, 020145-1–020145-10; https://doi.org/10.1063/1.5138878
Published by AIP Publishing. 978-0-7354-1938-4/$30.00

frictionless pivot while separating the torque motor from the hydraulic fluid. These valves can have an electrical feedback or a mechanical feedback, with the latter being more common in aerospace applications [2]. Deflector jet servovalves are more used in aerospace by virtue of their safe failure mode, while double nozzle flapper servovalves are more used in industry; jet pipe servovalves have higher costs, which hinder their diffusion. Compared to proportional valves [3-6], these valves present better dynamics by virtue of the two-stage assembly and the very low overlap at null.

Although the architectures of servovalves have not substantially changed for many years, they present a few disadvantages that are still unsolved. One of these drawbacks is represented by the fact that the flapper-flexure tube system can be affected by vibration, and a valve may experience failure of the thin-walled flexure-sleeve due to excessive bending under severe vibration or shock. In addition, lightly damped flapper resonance makes the valve main spool position very sensitive to external noise. To date, research studies in the scientific literature have mainly been focused on reduction of complexity of servovalves; in particular, a promising research field aims to replace the electromagnetic torque motor assembly with piezoelectric actuators, thus reducing complexity and manufacturing costs [7-13]. However, the scientific literature lacks proposals to reduce the undesired effects of external noise upon a servovalve. Only two very dated patents proposed two unusual geometries to reduce flapper vibration. The first one consisted in using an additional body with conical shape to be connected to the bottom of the flapper in order to damp vibrations [14]. The second one consisted in using additional chambers to be cut near the two nozzles surrounding the flapper (see fig.1) in order to act as dampers for the flapper [15]. However, to the best of our knowledge, these novel architectures have never been used in commercially available servovalves.

The underlying physics of the damping mechanism is not well-understood, and this problem has not been addressed in the scientific literature yet. Thus this research activity is focused on the analysis of the damping effect caused by the squeeze film inside the flapper-flexure tube system of servovalves. To this end, 3D CFD simulations with dynamic meshes are used. The main aim of this paper is to understand how damping forces are generated during flapper motion and where and how such forces act. In addition, the aim of this paper is to propose an effective CFD model which can be reproduced by companies and researchers to carry out further investigations aimed, for example, at assessing the effects of fluid properties and geometrical parameters upon the damping factor. The proposed model can also be used to explore new geometries for the flapper and the flexure tube that have the potential to enhance the squeeze film damping mechanism, thus enabling operation at increased vibration levels in future servovalves.

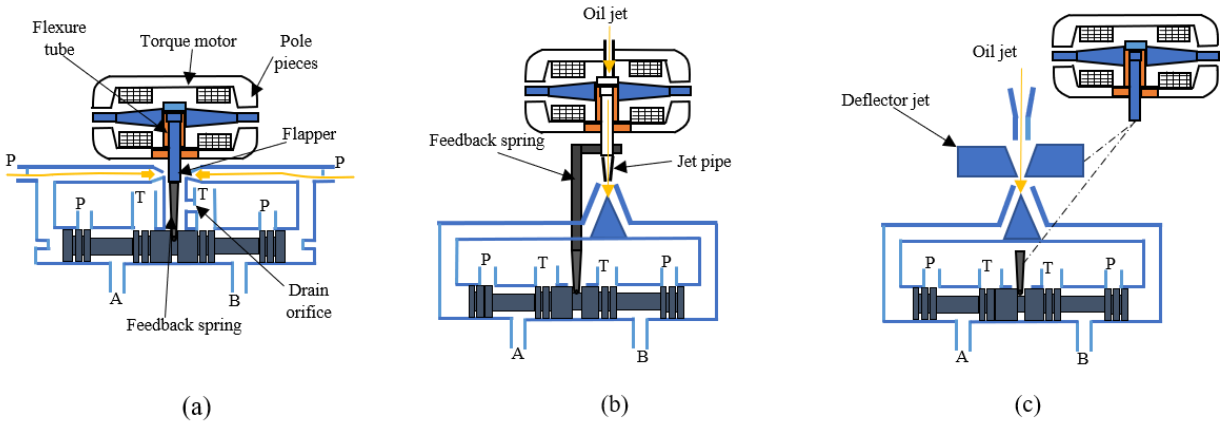

FIGURE 1. Operating principle of a double nozzle-flapper servovalve (a), jet pipe servovalve (b), and deflector jet servovalve (c), all with mechanical feedback [2]

COMPUTATIONAL GRID AND MODELLING

Ansys Workbench and Ansys Fluent were used to create the CFD model of the squeeze film inside a flapper-flexure tube system [16]. Real dimensions were used in this analysis; specifically, the same dimensions as those employed in servovalves manufactured by Moog for fuel control in aircraft were adopted. Information regarding these dimensions is omitted in the present paper because it is intellectual property of Moog.

Fig. 2 (a) shows a schematic of the flapper-flexure tube system, which might be used in any of the valve types illustrated in Fig. 1. The flapper can move inside the flexure tube, and during its motion the film of liquid between

the flapper and the tube is squeezed, providing useful damping against vibrations that usually occur at high frequency during valve operation. The real geometry shown in Fig. 2 (a) can be simplified as shown in Fig. 2 (b). The simplified architecture consists of a fixed outer tube (flexure tube) and a moving inner tube (flapper), the latter rotating around a pivot point located at the top of the axis of symmetry of the system. Since the squeeze effect is due to the phenomena concerned with the liquid comprised between the flapper and the flexure tube, the outlet part of the system was simplified as shown in Fig. 2 (b). The geometry is symmetric, therefore only a half of the simplified geometry was modelled. Fig. 3 (c) shows the 3d model obtained, and Fig. 3 (d) shows the corresponding computational grid along with the boundary conditions used to perform the CFD simulations. In this regard, the flexure tube was defined as a fixed wall, whereas the flapper was defined as a moving wall rotating around the pivot point with an assigned angular velocity ω. The angular velocity was assumed equal to 20 rad/s, which is an average value for the angular velocity estimated by Moog during their experimental tests.

The boundary condition "symmetry" was assigned to the symmetry plane; the "symmetry" condition was used since it allows the extent of the computational domain to be reduced to a half of the overall physical system, thus halving the overall computational time. The condition "dynamic mesh" was assigned to the interior zones, to the symmetry plane and to the top wall, which means that the mesh was deformed in these zones to cope with the movement of the flapper. Among the dynamic mesh options provided by Fluent, the smoothing method was selected. With this method, the interior nodes of the mesh move according to the flapper motion, but the number of nodes and their connectivity does not change. In this way, the interior nodes "absorb" the movement of the boundary [16].

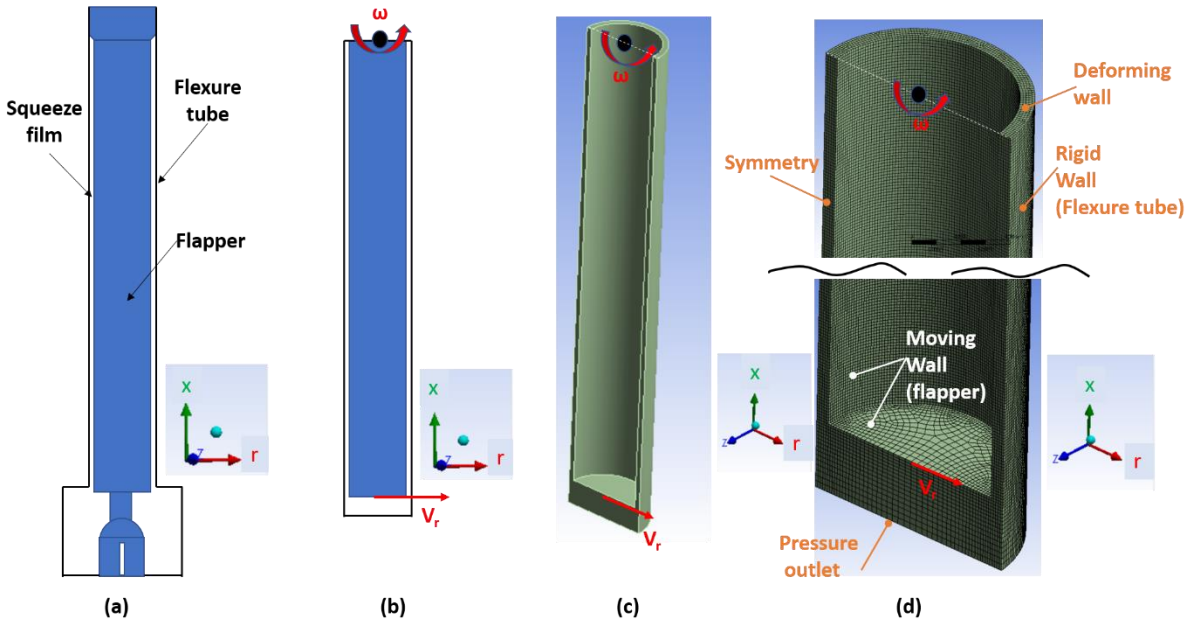

FIGURE 2. Schematization of a real architecture for the flapper-flexure tube system (a), simplified architecture (b), 3d model of a half of the simplified architecture (c), and computational grid of the 3d model (d)

The following conditions were set in the Fluent environment as far as the solver is concerned. The flow was treated as laminar and incompressible (i.e., with constant density ρ and constant dynamic viscosity μ). Specifically, the values of density and viscosity of Kerosene at 40 °C were used in the simulations, namely, ρ=799 kg/m^3 and μ =0.0009 kg m^{-1}s^{-1}, as would be suitable if the valve were used for aero engine fuel control. The pressure-based solver was used since the flow was considered incompressible.

The transient calculation was performed with a sufficiently low time step, namely Δt =0.00001 s, with 50 iterations per time step, and with 28 overall time steps necessary to cover the entire displacement of the flapper. At each time step, the grid was compressed by the smooth method to cope with the flapper motion. The maximum displacement was reached at the last time step; the maximum displacement in the real system is due to a mechanical stop present in the torque motor assembly.

The SIMPLE method was used for the pressure-velocity coupling, with PRESTO! for pressure spatial discretization, and second order upwind for spatial discretization of momentum [5]. The Fluent default under-relaxation factors were maintained, namely, 0.3 for pressure and 0.7 for momentum.

Fluent was able to predict the force acting on the flapper in the radial direction F_r (see coordinate systems in Fig.2) as the sum of the pressure forces and the viscous forces acting on the flapper surface. Subsequently, the damping factor C was calculated as follows:

$$C = \frac{F_r}{V_r} = \frac{F_r}{\omega L} \tag{1}$$

where V_r is the velocity at the flapper tip (bottom of the flapper) and L is the overall length of the squeeze film. Table 1 reports the main assumptions and parameters of the numerical model to facilitate an easy reproduction of the model.

TABLE 1. Parameters and setting of the numerical model

Boundary conditions	
Flapper	*Moving wall rotating around the pivot point with ω=20 rad/s*
Flexure tube	*Fixed wall*
Bottom outlet	*Pressure outlet (1 bar)*
Top	*Deforming wall*
Plane of symmetry	*Symmetry*
Interior region	*Interior with deforming mesh*
Pivot point	*Point located at the top of the axis of symmetry*
Dynamic mesh parameters	
Deforming Mesh Method	*Smoothing/diffusion*
Fluid setting	
Turbulence condition	*Laminar*
Compressibility	*Incompressible*
Density	ρ*=799 kg/m*^{3}
Viscosity	μ *=0.0009 kg/(ms)*
Solver setting	
Solver	*pressure-based transient*
Number of time steps	*28*
Duration of a time step	*0.00001 s*
Iterations per time step	*50*
Pressure-velocity coupling	*Simple*
Pressure discretization	*PRESTO!*
Momentum discr.	*second order upwind*
Pressure under-relaxation factor	*0.3*
Momentum under-relaxation factor	*0.7*

RESULTS

In this section, at first the grid convergence study aimed at selecting a proper computational grid, capable of ensuring both good accuracy and low computational time at the same time, is described. Then, the comparison between the numerical predictions and available experimental data is provided. Finally, the numerical predictions are analyzed in detail, showing the contours of Courant number, Reynolds number, static pressure and velocity magnitude. The analysis of these variables is instrumental in understanding how the damping forces are generated during the flapper motion.

Grid independence analysis

A grid independence analysis was performed to properly select the grid size. Six computational grids were generated, namely, with 2 100 000 cells (grid 1), 875 000 cells (grid 2), 465 000 cells (grid 3), 282 000 cells (grid 4), 140 000 cells (grid 5), and 63 000 cells, (grid 6). The damping factor calculated at the last time step was used to compare the six grids.

Among the six computational grids, grid 4 was selected since it provides the best compromise between accuracy and computational time. Fig.3 reports the plot of the scaled residuals achieved for the selected grid (grid 4). It can be

noted that at each time step a very high level of convergence was achieved, with all the scaled residuals being below 10^{-5}.

TABLE 2. Comparison among the six computational grids used for the grid independence analysis

Computational grid	Overall number of cells	Cells along r axis in the clearance of the squeeze film	Damping factor at the last time step C[Ns/m]
Grid 1	2 100 000	10	0.156
Grid 2	875 000	8	0.156
Grid 3	465 000	6	0.153
Grid 4	282 000	5	0.149
Grid 5	140 000	4	0.134
Grid 6	63 000	3	0.124

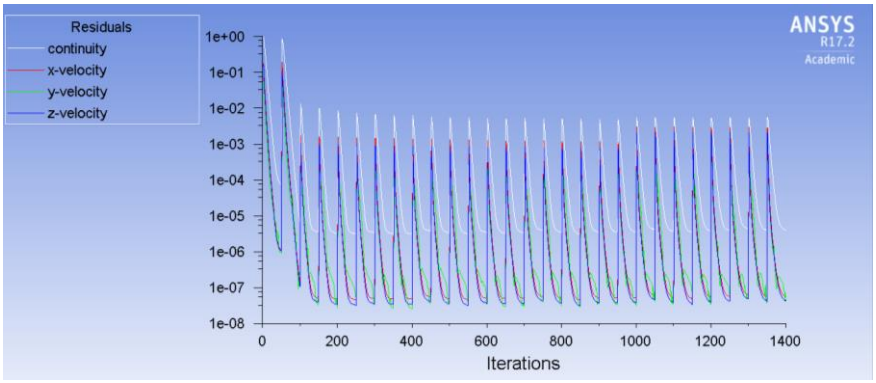

FIGURE 3. Scaled residuals vs number of iterations for grid 4

Experimental validation

The damping factor was experimentally retrieved by Moog for a flapper-flexure tube system having the same geometrical parameters as those employed in the present work. The fluid properties (temperature, density and viscosity) were the same as those employed in the numerical simulations. The experimental tests performed by Moog allowed the average damping factor to be estimated for an average velocity of the flapper tip. The average velocity of the flapper was 0.27 m/s, which corresponds to an angular velocity of 20 rad/sec, namely, the same angular velocity employed in the simulations.

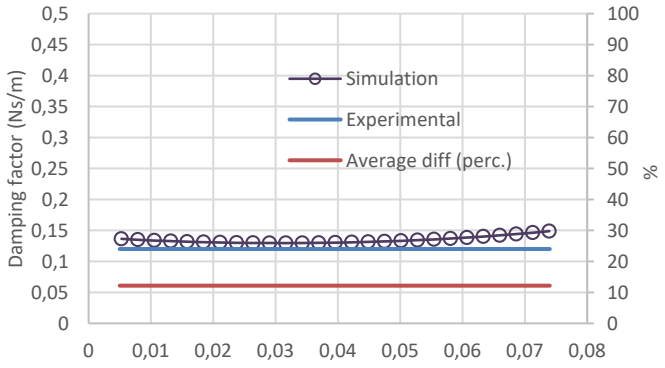

FIGURE 4. Experimental damping factor vs numerical damping factor

Fig. 4 compares the average experimental damping factor with the damping factor predicted by the simulations along the entire flapper displacement. As shown by the graph in Fig. 4, the average difference between the numerical predictions and the experimental damping factor is of the order of 10%.

Analysis of the numerical predictions

Fig. 5 shows the Courant number predicted on the symmetry plane and on three section planes perpendicular to the symmetry plane, both for a half of the maximum displacement of the flapper (Fig. 5a) and for the maximum displacement of the flapper (Fig.5b). The Courant number was calculated as:

$$CN = \frac{V\,\Delta t}{\Delta x} \tag{2}$$

where V is the velocity magnitude, Δt is the time-step, and Δx is the spacing of the grid. As shown by the contours in Fig.5, the Courant number is less than 1 throughout the fluid domain (except for a small percentage of cells, for which the Courant number is around 1), guaranteeing the stability of the computation for the chosen time step [16].

Fig.6 shows the contours of Reynolds number calculated on the symmetry plane and on the three section planes, both for a half of the maximum displacement of the flapper (Fig. 6a) and for the maximum displacement of the flapper (Fig.6b). The Reynolds number was calculated as follows:

$$R_e = \frac{V\,d\,\rho}{\mu} \tag{3}$$

where d is the clearance between the flapper and the flexure tube, which varies with the flapper motion. As shown by the contours of the Reynolds number, its value is below 200 throughout the squeeze film, with the maximum values occurring at the bottom of the squeeze film. These low values justify the assumption of laminar flow inside the squeeze film.

Fig. 7 and Fig. 8 show, respectively, the contours of static pressure and the vectors of velocity predicted on the symmetry plane and on the three section planes at a half of the flapper displacement (7a and 8a) and at the maximum flapper displacement (7b and 8b). These contours reveal how the damping factor is generated inside the squeeze film. Specifically, the movement of the flapper to the right creates restrictions on the right-hand side and enlargements on the left-hand side of the squeeze film. Because of this, the fluid is forced to move from the right to the left along the circumferential path. While moving from the right to the left, the fluid experiences a sudden restriction in the flow passage; at these low values of the Reynolds number, the internal shear forces resulting from the fluid viscosity causes a pressure drop along the circumferential path of the fluid, with the pressure on the right-hand side being higher than the pressure on the left-hand side of the squeeze film. In addition, part of the fluid is discharged from the right-hand side of the squeeze film to the outlet (bottom of the fluid domain defined as pressure outlet), whilst a part of the fluid comes from the outlet and enters the squeeze film on the left-hand side. As a result of all these fluid phenomena, the pressure acting on the flapper is higher on the right-hand side than the left-hand side, thus causing an overall force which opposes the flapper motion. This is the damping force caused by the squeeze film, which generates a beneficial effect in that it can damp the vibration of the flapper caused by external noise.

The contours of pressure in Fig. 7 also reveal that the pressure difference between the two sides of the squeeze film is not uniform along the flapper length; instead, the pressure difference is higher in the lower part of the squeeze film, and then it decreases gradually along the flapper length towards the top of the squeeze film. This is due to the fact that the flapper rotates around the pivot point placed at the top of the domain, therefore the film of oil is more "squeezed" in the bottom part than in the top part of the squeeze film.

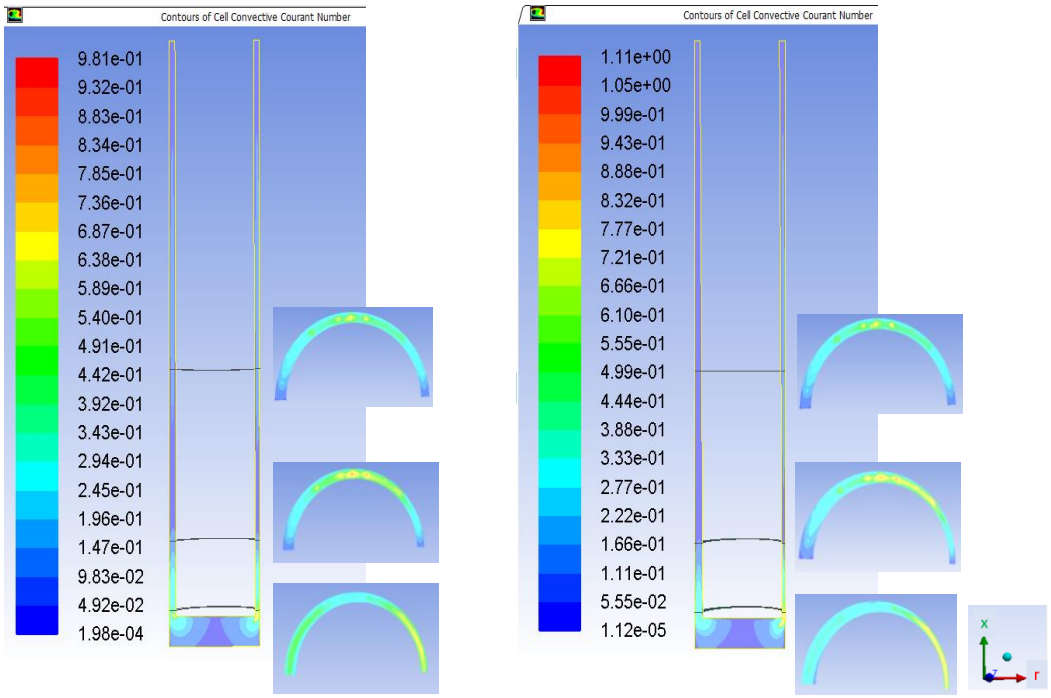

FIGURE 5. Contours of Courant number predicted at a half of the flapper displacement (a) and at the maximum flapper displacement (b)

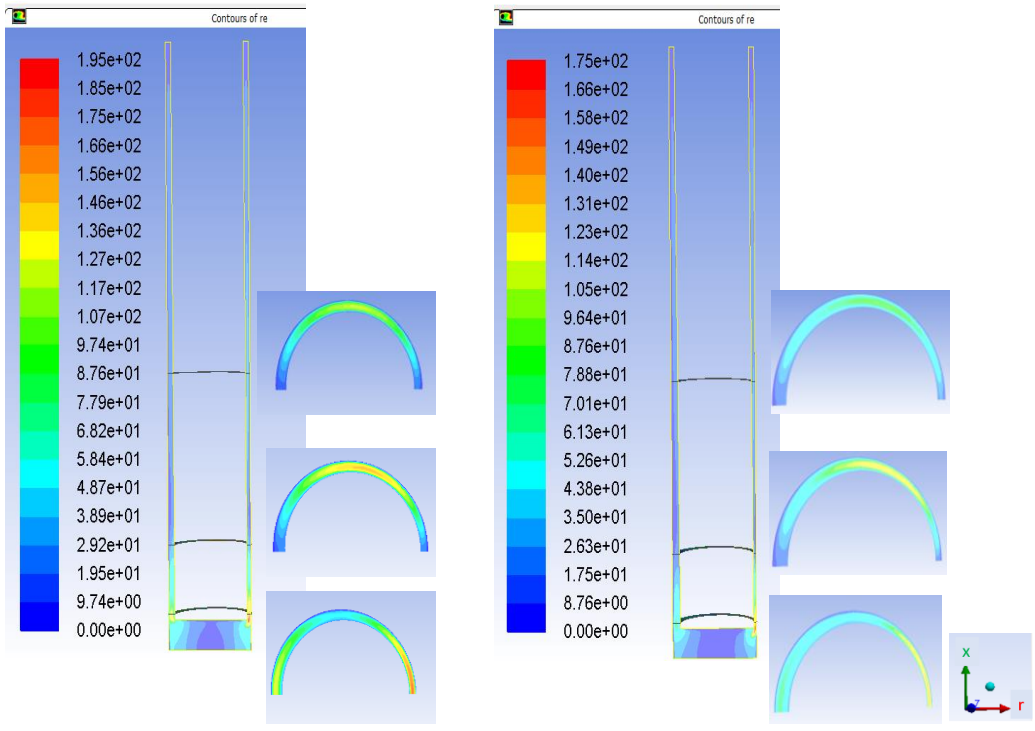

FIGURE 6. Contours of Reynolds number predicted at a half of the flapper displacement (a) and at the maximum flapper displacement (b)

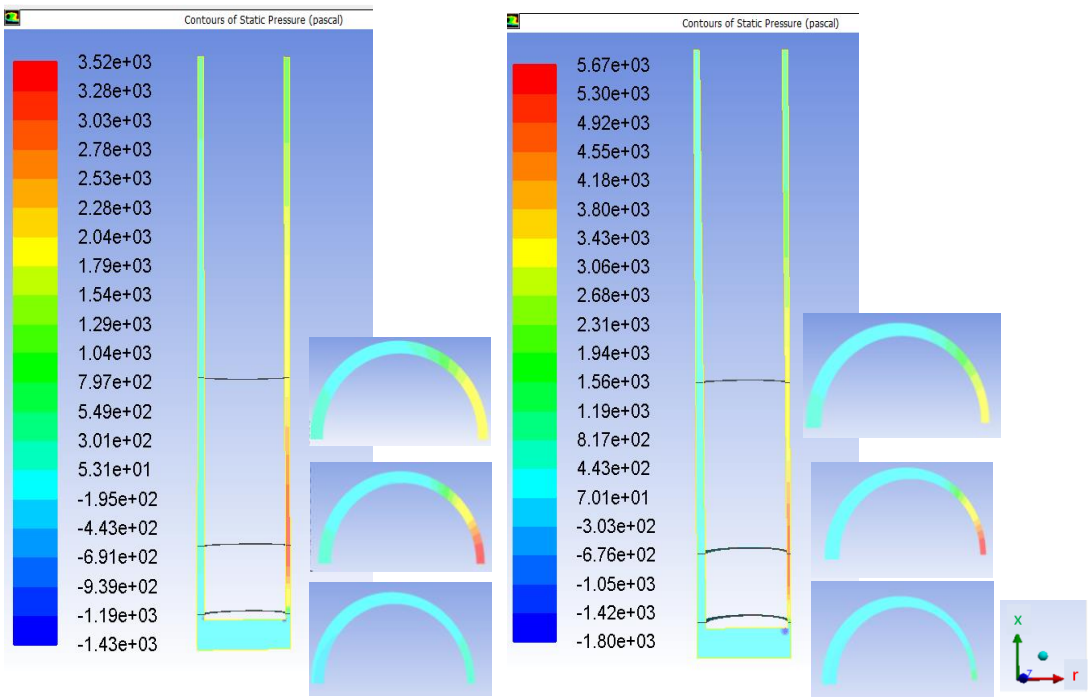

(a) (b)

FIGURE 7. Contours of static pressure (pascal) predicted at a half of the flapper displacement (a) and at the maximum flapper displacement (b)

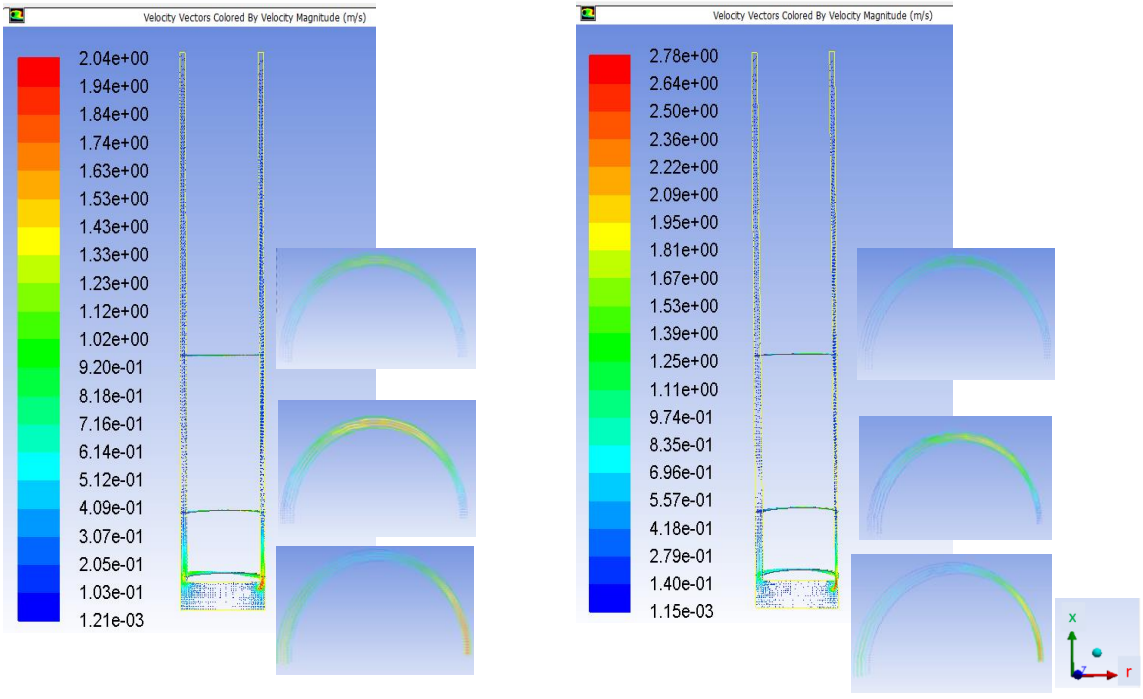

(a) (b)

FIGURE 8. Velocity vectors (m/s) predicted at a half of the flapper displacement (a) and at the maximum flapper displacement (b)

The proposed model lays the basis for further investigations into the damping mechanism generated by the squeeze film. Specifically, the proposed CFD model can be used to:

- assess the effects of fluid properties (density and viscosity) upon the damping factor;
- assess the effects of different flapper velocities upon the damping factor;
- assess the effects of different lengths and clearances upon the damping factor;
- find different flapper and flexure tube profiles that can enhance the damping factor.

These analyses could be instrumental in enabling operation at increased vibration levels on future servovalves, thus improving their performance.

CONCLUSIONS

For the first time, this paper developed a CFD model of the squeeze film inside the flapper-flexure tube system employed in two-stage servovalves. Existing dimensions of a typical Moog's flapper-flexure tube system were used in the analysis. The CFD model allowed understanding where and how the damping forces are generated during the movement of the flapper inside the flexure tube, providing detailed contours of the main variables, such as Courant number, Reynolds number, static pressure and velocity. It was shown that the flapper movement creates restrictions on one side and enlargement on the other side of the squeeze film. At such low Reynolds numbers, the viscosity effects are predominant, and they generate a pressure drop between the two sides of the squeeze film because of internal friction. This difference in pressure determines an overall force acting on the flapper which opposes the flapper motion, providing useful damping. It was also shown that this damping force is maximum at the bottom of the squeeze film and decreases at the center and top of the squeeze film.

The proposed model can be easily reproduced to help manufacturers understand the effects of fluid properties and geometrical dimensions upon the damping factor. These aspects will be investigated in forthcoming work, with the aim to enable operation of servovalves at increased vibration levels.

REFERENCES

1. Plummer, A. R., "Electrohydraulic servovalves – past, present, and future," 10th Int. Fluid Power Conf., pp. 405–424, 2016.
2. Tamburrano, P., Plummer, A. R., Distaso, E., & Amirante, R. (2018). A review of electro-hydraulic servovalve research and development. International Journal of Fluid Power, 1-23.
3. Tamburrano, P., Plummer, A. R., Distaso, E., & Amirante, R. (2019). A Review of Direct Drive Proportional Electrohydraulic Spool Valves: Industrial State-of-the-Art and Research Advancements. Journal of Dynamic Systems, Measurement and Control, Transactions of the ASME 141(2), 020801.
4. Amirante, R., Distaso, E., & Tamburrano, P. (2016). Sliding spool design for reducing the actuation forces in direct operated proportional directional valves: Experimental validation. Energy Conversion and Management, 119, pp. 399-410
5. Amirante, R., Distaso, E., & Tamburrano, P. (2014). Experimental and numerical analysis of cavitation in hydraulic proportional directional valves. Energy Conversion and Management, 87, pp. 208-219
6. Amirante, R., Catalano, L. A., Poloni, C., & Tamburrano, P. (2014). Fluid-dynamic design optimization of hydraulic proportional directional valves. Engineering Optimization, 46(10), pp. 1295-1314.
7. J. Jeon et al. "A new type of a direct-drive valve system driven by a piezostack actuator and sliding spool," Smart Mater. Struct., vol. 23, no. 7, 2014.
8. S. Karunanidhi and M. Singaperumal, "Mathematical modelling and experimental characterization of a high dynamic servo valve integrated with piezoelectric actuator," Proc. Inst. Mech. Eng. Part I J. Syst. Control Eng., vol. 224, no. 4, pp. 419–435, 2010.
9. Milecki A. Modelling and investigation of electrohydraulic servovalve with piezo element. Proc Inst Mech Technol 2006; 26: 181–188.
10. Bertin, M. J. F., Plummer, A. R., Bowen, C. R., Johnston, D. N., & City, S. (2014, September). An investigation of piezoelectric ring benders and their potential for actuating servo valves. In Proceedings of the Bath/ASME symposium on fluid power and motion control (Vol. 6).

11. Tamburrano, P., Amirante, R., Distaso, E., & Plummer, A. R. (2018). Full simulation of a piezoelectric double nozzle flapper pilot valve coupled with a main stage spool valve. Energy Procedia, 148, pp. 487-494
12. J Persson, L. J., Plummer, A. R., Bowen, C. R., & Brooks, I. (2015, October). Design and modelling of a novel servovalve actuated by a piezoelectric ring bender. In ASME/BATH 2015 Symposium on fluid power and motion control (pp. V001T01A043-V001T01A043). American Society of Mechanical Engineers.
13. Tamburrano, P., Amirante, R., Distaso, E., and Plummer, A.R. (2018). A Novel Piezoelectric Double-Flapper Servovalve Pilot Stage: Operating Principle and Performance Prediction. In Bath/ASME Symposium on Fluid Power and Motion Control FPMC 2018, 12 - 14 September 2018, University of Bath, Bath (UK).
14. J.R. Sjolund, Jan. 8, 1985. Nozzle And Flapper With Film Squeeze Damping. Patent 4492245.
15. R.K. Hedlund, February 11, 1969. Vibration damping nozzle and flapper. Patent 3426970.
16. ANSYS FLUENT Theory Guide 14.0. November 2011. Fluent Inc.